

Raman Spectroscopy of Free-Standing Individual Semiconducting Single-Wall Carbon Nanotubes

M. Paillet,* S. Langlois, and J.-L. Sauvajol

Laboratoire des Colloïdes, Verres et Nanomatériaux (UMR CNRS 5587), Université Montpellier II, 34095 Montpellier Cedex 5, France

L. Marty, A. Iaia, C. Naud, V. Bouchiat, and A. M. Bonnot

LEPES, Centre National de la Recherche Scientifique, BP166X, F-38042 Grenoble Cedex 9, France

Received: March 30, 2005; In Final Form: November 9, 2005

The radial breathing modes and tangential modes have been systematically measured on a large number of individual semiconducting single-wall carbon nanotubes (thin bundles) suspended between plots (free-standing single-wall carbon nanotubes). The strong intensity of the Raman spectra ensures the precision of the experimentally determined line shapes and frequencies of these modes. The diameter dependence of the frequencies of the tangential modes was measured. This dependence is discussed in relation with recent calculations. The present data confirm/contradict some previous interpretations.

I. Introduction

The resonant Raman-scattering technique is a powerful tool for investigating single-wall carbon nanotubes (SWCNTs), for which the radial breathing mode (RBM), usually in the 100–300 cm^{-1} range, and the tangential modes (TM), usually in the 1400–1700 cm^{-1} range, are the two main features. Raman spectroscopy has been widely used to study and characterize SWCNT bundles. Especially, it was found that the measurement of the RBM frequencies provides an efficient method to determine the diameters of the tubes present in SWCNT bundles.^{1–3} On the other hand the profile of the TM band depends on the semiconducting or metallic character of the tube. An explicit Breit–Wigner–Fano (BWF) profile of the TM band in SWCNT bundles is usually taken as an indication for the metallic character of the tubes.^{4–7} The BWF intensity is expected to decrease strongly in individual SWCNTs.⁸ Recently, we have shown the vanishing of the BWF component in well-localized individual and isolated metallic SWCNTs at a given excitation energy. This result allows us to conclude that a semiconducting-like profile can also feature an individual metallic SWCNT.⁹

The dependence of the resonant Raman spectrum with the excitation energy is usually understood in the framework of a single resonance process,¹ and all the modes are assumed to be Γ -point modes. It was also proposed that the Raman spectrum of SWCNTs originate from a double resonance process with phonon wavevector $q > 0$.¹⁰ Obviously, the study of individual SWCNTs by Raman spectroscopy is needed to clarify this debate. The aim of the present paper is to report new Raman data obtained on individual suspended (free-standing) carbon nanotubes growth by the hot filament assisted chemical vapor deposition technique. These data confirm/contradict some previous interpretations.

II. Experimental Section

Suspended SWCNTs have been self-assembled between Si pillars with a top 2 nm Co layer using the hot filament assisted

chemical vapor deposition (CVD) technique.¹¹ By this route a large majority of free-standing individual SWCNTs is prepared. However free-standing thin bundles are also present in the sample.¹² The average length of the tubes, determined by the interdistance between Si pillars, was about 40 nm. Figure 1 shows an image of such a nanotube.

Room-temperature Raman spectra were obtained using a triple subtractive Jobin-Yvon T64000 spectrometer equipped with a liquid nitrogen cooled charge coupled device (CCD) detector. The Raman spectra were collected in a backscattering configuration by a microscope using a 100 \times objective (laser spot ~ 1.5 μm). The instrumental resolution was 2 cm^{-1} . The 488 nm (2.54 eV), 514.5 nm (2.41 eV), and 647.1 nm (1.92 eV) lines from an Ar/Kr laser were used. The power impinging on the sample was ~ 200 μW . A precise and reproducible positioning of the tubes under the laser spot was monitored with a piezoelectric nanopositioner. The orientation of the tube axis (the Z axis) with respect to the polarization of the incident (scattered) light is unknown.

III. Results

In contrast with previous investigations devoted to Raman spectroscopy at the single nanotube level, our study presents two specificities: (i) systematically RBM and TM are measured on each investigated free-standing individual SWCNT (thin bundle); (ii) as expected,¹³ the Raman spectra recorded on suspended SWCNTs have a strong intensity, the RBM and TM line shapes are well-defined, and the frequencies of the Raman active modes are known with a good accuracy.

In the TM range, the usual group theory predicts six Raman active modes for a chiral nanotube (two A, two E₁, two E₂), and three for an achiral (armchair, zigzag) nanotube (one A_{1g}, one E_{1g}, one E_{2g}).¹⁴ Recently, the dependence of a nonresonant Raman spectrum has been calculated as a function of the chirality for nanotubes of similar diameters (for instance, see Figure 3 in ref 15). For each symmetry, one labels ω_z and ω_a the TM frequency of the zigzag and armchair SWCNT,

* Current e-mail address: matthieu.paillet@umontreal.ca.

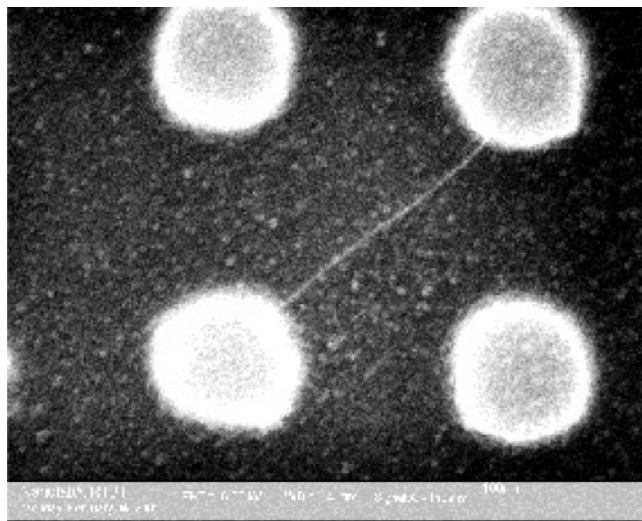


Figure 1. A scanning electron microscopy image showing a suspended nanotube prepared by using the hot filament assisted chemical vapor deposition technique.

respectively. The increase of the chiral angle (θ) from 0 to 30° leads to the appearance of two peaks at frequencies close to ω_z and ω_a . The intensity of these peaks shifts from the one located around ω_z to that located around ω_a when increasing θ . For the armchair tube ($\theta = 30^\circ$), a single peak located at ω_a has nonzero intensity. It is found that the lowest frequency component has $E_{2g}(\text{LO})$ symmetry for zigzag SWCNT, while for armchair SWCNTs the $E_{2g}(\text{TO})$ symmetry is found to have the highest frequency. For chiral tubes, the LO or TO character of the modes, in the strict sense, is lost. However, by continuity, the LO and TO notations are generally used also for chiral tubes. The vicinity of the calculated frequencies of $A(A_{1g})$ and $E_1(E_{1g})$ tangential modes can be pointed out. For the 1.37 nm (10,10) armchair SWCNT, the $A_{1g}(\text{TO})$ is calculated at 1582 cm^{-1} and the $E_{1g}(\text{LO})$ at 1580 cm^{-1} . For the 1.35 nm (17,0) zigzag SWCNT, the $A_{1g}(\text{LO})$ mode is located at 1586 cm^{-1} and the $E_{1g}(\text{TO})$ mode at 1582 cm^{-1} . These results highlight the difficulty of experimentally resolved $A(A_{1g})$ and $E_1(E_{1g})$ modes, as discussed in ref 16. Recent ab initio calculations also show that $A(A_{1g})$ and $E_1(E_{1g})$ modes have rather similar frequencies, especially, the $A(A_{1g})(\text{LO})$ and $E_1(E_{1g})(\text{TO})$ almost coincide for semiconducting tubes.¹⁷ Depending on the polarization scattering geometry (direction of the polarization of the incident (scattered) light with respect to the direction of the nanotube axis) and resonance conditions, two, four, or six lines are expected in the TM range of a chiral tube.^{14,15} The dependence of the Raman spectrum with the size of the bundles has been calculated.^{18,19} Concerning the TM of semiconducting tubes, no significant change is observed for tubes in bundles with regards to individual tubes: the number of lines is the same and the frequency of the modes are only slightly upshifted.

In the following are reported Raman spectra recorded on free-standing carbon nanotubes. The frequency and full width at half-maximum (in brackets) of the RBM and TM have been obtained from the fit of the spectra by assuming a Lorentzian line shape for each mode. With the 2.41 eV laser excitation ($\lambda = 514.5$ nm) the Raman spectra of a first series of three individual SWCNTs of similar diameters have been measured. A strong single line appears in the RBM range (Figure 2). It is located at 181 cm^{-1} (4.5 cm^{-1}) for the first nanotube (Figure 2.a1) and around 179 cm^{-1} for the second (4.5 cm^{-1}) and third (5.5 cm^{-1}) SWCNT of this series (parts b1 and c1 of Figure 2). Recently, by combining Raman spectroscopy and electron diffraction

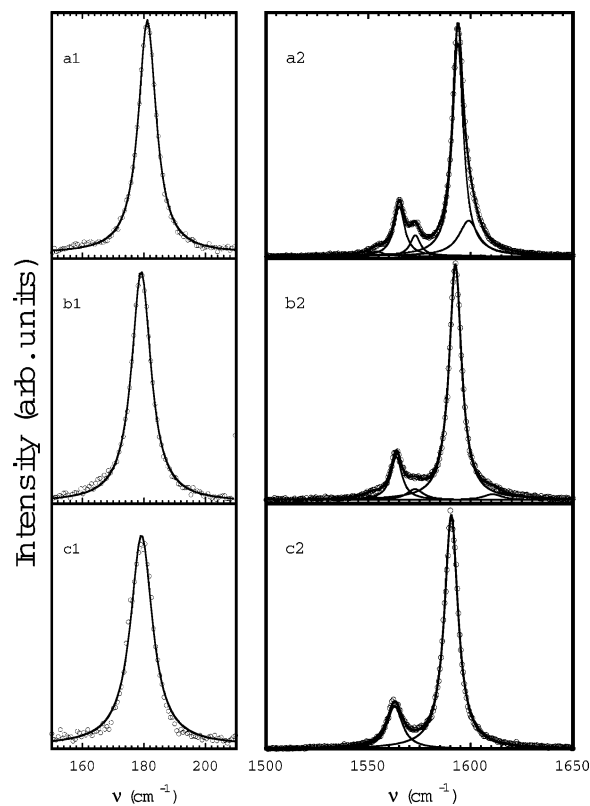


Figure 2. RBM (left) and TM (right) parts of the Raman spectra from three individual SWCNTs measured using $E_{\text{laser}} = 2.41$ eV (514.5 nm): experimental data (open dots); each component of RBM and TM bunch is fitted by a Lorentzian profile (thin solid line); calculated total profile (thick solid line).

experiments on the same free-standing individual SWCNTs, we have derived in a broad diameter range (from 1.4 to 3 nm) the expression that relates the tube diameter to the RBM frequency: $\nu(\text{cm}^{-1}) = 204 (\text{nm cm}^{-1})/d (\text{nm}) + 27 (\text{cm}^{-1})$.²⁰ It must be emphasized that this relation is in reasonable agreement with those previously established for SWCNTs deposited on a substrate,²¹ or wrapped in a surfactant,^{22,23} in the common diameter range (i.e., from 1.4 to 1.7 nm).²⁰ This agreement suggests that the RBM frequency is not strongly affected by the environment. By use of this latter relation, the diameter of the three tubes of this first series is evaluated around 1.33 nm. With regards to the resonance conditions,⁵ the three tubes are expected to be semiconducting, and in resonance with the E_{33}^S transition. The TM bunch measured on the first individual SWCNT of this series displays five components (Figure 2.a2). As a consequence, it features a chiral tube. Well-resolved lines located at 1565 cm^{-1} (4.3 cm^{-1}) and 1573 cm^{-1} (4 cm^{-1}) are observed and assigned to $A(\text{TO})$ and $E_1(\text{LO})$ modes, respectively.^{16,24} The dominant component is centered at 1593.5 cm^{-1} (4.5 cm^{-1}) and assigned to the unresolved $A(\text{LO}) + E_1(\text{TO})$ doublet. Finally, two shoulders appear on the low-frequency side (1554 cm^{-1} (5 cm^{-1})) and high-frequency side (1599 cm^{-1} (9.5 cm^{-1})) of the TM bunch, and they are attributed to $E_2(\text{LO})$ and $E_2(\text{TO})$ phonon modes, respectively. The observation of E_2 modes indicates that the tube is not along the laser polarization, and the (XX) component of the polarizability tensor (incident and scattered light polarized crossed with nanotube axis) is active in our experimental configuration. The TM bunch of the second SWCNT is well fitted by five Lorentzians centered around 1551.5 cm^{-1} (5.5 cm^{-1}) ($E_2(\text{LO})$), 1563.5 cm^{-1} (4.6 cm^{-1}) ($A(\text{TO})$), 1573 cm^{-1} (7.5 cm^{-1}) ($E_1(\text{LO})$), 1592.5 cm^{-1} (5.3 cm^{-1}) ($A(\text{LO}) + E_1(\text{TO})$), and

1610.5 cm^{-1} (fwhm = 9 cm^{-1}) (Figure 2.b2). It is tempting to assign this latter line to $E_2(\text{TO})$ phonon mode. However, the frequency of this line is higher than the frequency of the $E_2(\text{TO})$ phonon mode predicted by the different calculations and usually found in experiments (close to 1600 cm^{-1}). In graphite and multiwall carbon nanotubes, a band around 1620 cm^{-1} , the so-called D'-band, was assigned to a defect-induced mode.^{25,26} A Raman band was also observed in the same range in SWCNTs, and it was well established as a defect-induced double resonance feature.²⁷ A band around 1610 cm^{-1} was also found in an highly disordered fiber of SWCNT.²⁸ As a consequence, the 1610.5 cm^{-1} component is assigned as a defect-induced mode. In agreement with this assignment, a D-band was also observed in the same spectrum. Measurement of the excitation profile of this band will allow precise determination of its origin. The TM bunch of the third SWCNT is described by using only two dominant Lorentzian components (Figure 2.c2). These components are located at 1563 cm^{-1} (7 cm^{-1}) and 1590.5 cm^{-1} (6 cm^{-1}), and assigned to unresolved $A(\text{TO}) + E_1(\text{LO})$ and $A(\text{LO}) + E_1(\text{TO})$ modes, respectively. In the present Raman experiment, the conditions of polarization of the incident and scattered lights with respect to the nanotube axis are unknown, and they are certainly different from one tube to the other. That can explain the changes in the relative intensity of the peaks in the different spectra. However, differences in the polarization conditions cannot explain the weak but significant changes in the peak positions for tubes of similar diameters. Two explanations can be proposed for this result: (i) Because thin bundles have been observed in our sample,¹² some measurements could be performed on thin bundles and other on individual SWCNTs. As previously recalled, the interaction between tubes leads to an upshift of the modes with respect to their position in individual SWCNTs. This could explain the differences of the frequency of TM observed on these different samples. (ii) On the other hand, this result could indicate the sensitivity of the frequencies of the tangential modes with the chiral angle θ . However, in this assumption, the present Raman data do not allow knowing the value of this angle, and then the (n,m) indices of the tube.

Panels a1–b2 of Figure 3 show the Raman spectra measured on a second series of SWCNTs using the 2.41 eV excitation. These two semiconducting SWCNTs are featured by a single narrow RBM located at 173.5 cm^{-1} (4 cm^{-1}) and 173.5 cm^{-1} (5.5 cm^{-1}), respectively ($d \approx 1.39$ nm) (Figure 3.a1 and 3.b1). They are in resonance with the E_{33}^S transition. The TM profile of the first SWCNT (Figure 3.a2) shows a first group of well-defined lines of similar intensities located at 1553 cm^{-1} (5.5 cm^{-1}), 1563 cm^{-1} (4.5 cm^{-1}), and 1573.5 cm^{-1} (9 cm^{-1}), and a dominant component located at 1599 cm^{-1} (11.5 cm^{-1}). A broad shoulder at 1611.5 cm^{-1} (13 cm^{-1}) and a weak sideband at 1533 cm^{-1} (5 cm^{-1}) are also measured. The TM bunch of the second SWCNT displays six Lorentzian components (Figure 3.b2). The strongest mode is located at 1596.5 cm^{-1} (10.5 cm^{-1}). Two narrow peaks, clearly resolved, are observed at 1566 cm^{-1} (5 cm^{-1}) and 1572.5 cm^{-1} (3.5 cm^{-1}). Finally, two shoulders appear on the low-frequency side (1556 cm^{-1} (7 cm^{-1})) and high-frequency side (1610 cm^{-1}) of the TM bunch. For these two tubes, we can propose the following attribution: (i) the components around 1555 cm^{-1} are attributed to $E_2(\text{LO})$ phonon modes; (ii) the modes around 1597 cm^{-1} are the unresolved $A(\text{LO}) + E_1(\text{TO})$ doublets; (iii) the modes around 1566 and 1573 cm^{-1} are the resolved $A(\text{TO})$ and $E_1(\text{LO})$ modes, respectively. The 1533 and 1610 cm^{-1} lines are assigned as defect-induced double resonance features.^{27,28} It must be pointed

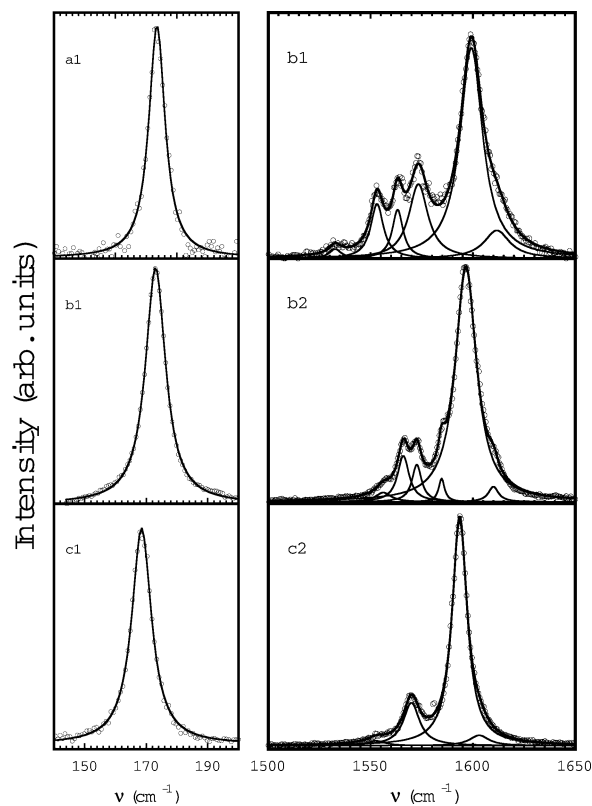


Figure 3. RBM (left) and TM (right) parts of the Raman spectra from three individual SWCNTs: experimental data (open dots); each component of RBM and TM bunch is fitted by a Lorentzian profile (thin solid line); calculated total profile (thick solid line). The Raman spectra of the two first individual SWCNTs are measured using $E_{\text{laser}} = 2.41$ eV (514.5 nm), and the spectrum of the third individual SWCNT is measured using $E_{\text{laser}} = 2.54$ eV (488 nm).

out that a weak line at 1585 cm^{-1} (2 cm^{-1}) is also observed in the TM bunch of the second SWCNT of this series. Figure 3.c1–c2 shows the Raman spectrum, measured using the laser excitation $E_1 = 2.54$ eV ($\lambda = 488$ nm), on an individual SWCNT featured by a single RBM at 168.5 cm^{-1} (5 cm^{-1}) ($d \approx 1.44$ nm) (Figure 3.c1). This SWCNT is in resonance with the E_{33}^S transition. The TM line shape (Figure 3.c2) is well fitted by using four Lorentzian components centered at 1552 cm^{-1} ($E_2(\text{LO})$), 1569 cm^{-1} (6.8 cm^{-1}) (unresolved $A(\text{TO}) + E_1(\text{LO})$), 1593 cm^{-1} (5.5 cm^{-1}) (unresolved $A(\text{LO}) + E_1(\text{TO})$), and 1603 cm^{-1} ($E_2(\text{TO})$), respectively.^{16,21,24}

The Raman spectra measured on two individual semiconducting SWCNTs, using the 1.92 eV laser excitation ($\lambda = 647.1$ nm) are reported on Figure 4. With regards to the resonance conditions, these two tubes are in resonance with the E_{33}^S transition. In the first spectrum a strong RBM is observed at 148 cm^{-1} (3 cm^{-1}) ($d \approx 1.68$ nm) with a weak shoulder at 141 cm^{-1} ($d \approx 1.79$ nm) (Figure 4.a1). The TM bunch has components at 1564 cm^{-1} (4.5 cm^{-1}) ($E_2(\text{LO})$), 1579 cm^{-1} (3.5 cm^{-1}) ($A(\text{TO}) + E_1(\text{LO})$ modes), and 1597.5 cm^{-1} (12 cm^{-1}) (unresolved $A(\text{LO}) + E_1(\text{TO})$ modes) (Figure 4.a2). The fit of the TM profile shows weak components located at 1586.5 cm^{-1} (6 cm^{-1}) and 1543.5 cm^{-1} (5 cm^{-1}). The concomitant observation of both these lines could be the signature of the presence of a metallic tube under the laser spot.²⁹ With regards to the resonance condition, the diameter of this metallic tube should be around 1.4 nm. However no RBM around 173 cm^{-1} was detected in our experiment. The TM bunch of the second SWCNT, featured by a single RBM at 143.5 cm^{-1} (9 cm^{-1}) ($d \approx 1.75$ nm) (Figure 4.b1) contains five components centered at

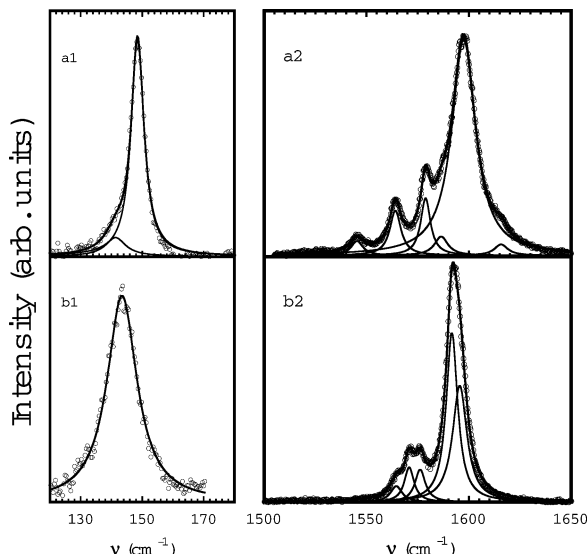


Figure 4. RBM (left) and TM (right) parts of the Raman spectra from two individual SWCNTs measured using $E_{\text{laser}} = 1.92$ eV (647.1 nm): experimental data (open dots); each component of RBM and TM bunch is fitted by a Lorentzian profile (thin solid line); calculated total profile (thick solid line).

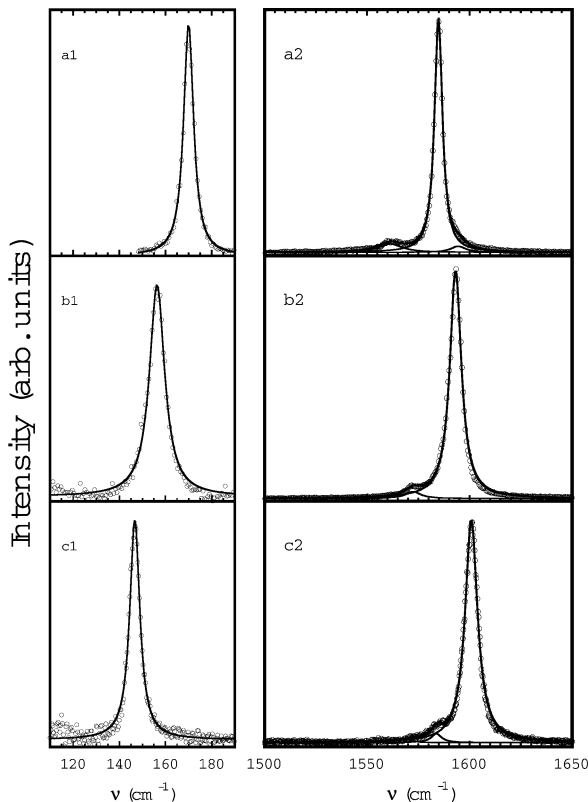


Figure 5. RBM (left) and TM (right) parts of the Raman spectra from three isolated SWCNTs: experimental data (open dots); each component of RBM and TM bunch is fitted by a Lorentzian profile (thin solid line); calculated total profile (thick solid line). The Raman spectra of the two first individual SWCNTs are measured using $E_{\text{laser}} = 2.41$ eV (514.5 nm), and the Raman spectrum of the third individual SWCNT is measured using $E_{\text{laser}} = 1.92$ eV (647.1 nm).

1564.5 cm^{-1} (5 cm^{-1}) ($E_2(\text{LO})$), 1571 cm^{-1} (4 cm^{-1}) and 1592 cm^{-1} (4.7 cm^{-1}) ($A(\text{TO})$ and $A(\text{LO})$ modes, respectively), and 1576 cm^{-1} (4 cm^{-1}) and 1595.5 cm^{-1} (6.5 cm^{-1}) ($E_1(\text{LO})$ and $E_1(\text{TO})$ modes, respectively) (Figure 4.b2).

In Figure 5 are reported the RBM and the TM ranges of three selected nanotubes which display the same TM line shape,

namely a strong single line (parts a2, b2, and c2 of Figure 5). In agreement with calculations,^{15,16} the spectrum, measured using the 2.41 eV excitation energy, and featured by a RBM at 156.5 cm^{-1} (5 cm^{-1}) ($d \approx 1.57$ nm) and a dominant 1593 cm^{-1} (4.8 cm^{-1}) $A(\text{LO})$ mode, could be attributed to the typical Raman response of a semiconducting SWCNT with a small chiral angle in resonance with the E_{44}^{S} transition (parts b1 and b2 of Figure 5). Concerning the spectrum, measured using the 1.92 eV excitation energy, and featured by the dominant line at 1601 cm^{-1} (5.2 cm^{-1}) (Figure 5.c2), it was previously suggested that this line could be assigned to E_2 symmetry mode.²⁴ Indeed a line, at a similar position, was observed with an intensity close to that of the 1591 cm^{-1} $A(\text{LO})$ mode in a polarized (XX) Raman spectrum (Figure 2 of ref 24). By contrast with this previous result, any A mode line located around 1591 cm^{-1} is observed in our spectrum where only a weak shoulder around 1585 cm^{-1} is found (Figure 5.c2). In addition, in the same experimental configuration, a strong RBM located at 147 cm^{-1} (fwhm = 2.5 cm^{-1}) ($d \approx 1.70$ nm), is observed (Figure 5.c1). Previous polarized Raman experiments performed on oriented SWCNTs have shown the same dependence of the intensity of the RBM and TM A symmetry modes with the orientation of the polarization of the incident light with respect to the nanotube axis, namely, a maximum of the intensity when the incident and scattered polarizations and the nanotube axis are along the same direction (ZZ component), and a minimum of the intensity for incident and scattered polarizations normal to the nanotube axis (XX component).^{30,31} As a consequence, and opposite to previous attributions,²⁴ this 1601 cm^{-1} line may be assigned to a $A(\text{LO})$ symmetry mode. Finally, concerning the strong line at 1585 cm^{-1} (2.8 cm^{-1}) (Figure 5.a2), the same discussion that the one done for the 1601 cm^{-1} line can be reproduced. The concomitant evidence of a strong RBM at 170 cm^{-1} (2.5 cm^{-1}) ($d \approx 1.43$ nm), suggests that the 1585 cm^{-1} line is a A symmetry mode of a semiconducting nanotube in resonance with the E_{33}^{S} transition. Weak lines around 1585 cm^{-1} were also observed in the low-frequency side of the intense components in two other spectra (Figures 3.b2 and 4.a2). That means that for the related experiments at least two tubes were located under the laser spot. In the following, we will come back to the assignment of the 1585 cm^{-1} mode.

IV. Discussion

The strong intensities of the radial breathing modes and tangential modes ensure the precision of the experimental line shape and frequency of all these modes. In the majority of the semiconducting tubes investigated here, the D band was undetectable. In a few tubes the D and D' (1610 cm^{-1}) components were observed. This result emphasizes the high crystallinity of the tubes prepared by the hot filament assisted CVD technique.¹¹ In the following the dependence of the TM on the diameter of the SWCNTs is discussed.

First we would like to discuss the striking results displayed in Figure 5. Because calculations predict that nanotubes with the same chiral angle display the same profile (see for instance refs 14 and 15), it is tempting to claim that these results show the pure diameter dependence of the TM frequencies of individual SWCNTs. In this assumption, the average dependence of the frequency of the dominant TM as a function of the diameter is approximately 70 cm^{-1}/nm . This value is significantly higher than that derived from the different calculations (between ≈ 1 and 20 cm^{-1}/nm) for tubes in the same diameter range. As a matter of fact this assumption can be ruled out. On the basis of the predictions of calculations,^{14,15,17} we can assume that the spectra dominated by a TM at high frequency are the intrinsic

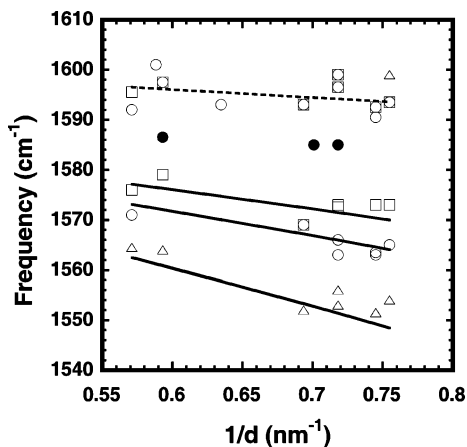


Figure 6. Dependence of the frequencies of the tangential modes as a function of the inverse of the diameter for the series of individual SWCNTs discussed above. A symmetry modes (open dots), E_1 symmetry mode (open squares), E_2 symmetry mode (open triangles), modes around 1585 cm^{-1} (full dots). The solid lines represent the best fit of the data of ref 24. The dashed line is a linear fit of the frequencies of the unresolved $A(\text{LO}) + E_1(\text{TO})$ TM.

Raman responses of a semiconducting SWCNT with a small chiral angle (close to a zigzag tube) (parts b and c of Figure 5) and that, conversely, the spectra dominated by a TM at low frequency are the intrinsic Raman response of a semiconducting SWCNT with a large chiral angle (Figure 5.a). The large majority of the spectra measured on about 50 individual tubes in this work, and the large majority of the spectra published in the literature, displays a dominant TM at high frequency ($>1590\text{ cm}^{-1}$). As a consequence, the assignment of the 1585 cm^{-1} line as the signature of a semiconducting SWCNT with a large chiral angle leads to the conclusion that the majority of semiconducting tubes prepared by different routes have a small chiral angle. This conclusion also seems to be unreasonable.

In Figure 6 is displayed the dependence of the high-frequency modes, previously assigned in terms of symmetry, as a function of the inverse of the diameter. On this plot, we compare our data (symbols in Figure 6) with the best fit of the data reported in ref 24 (solid line in Figure 6). A good agreement is found. Some remarks can be done: (i) First, we confirm the difficulty to resolve the high-frequency $A(\text{LO})$ and $E_1(\text{TO})$ phonon modes. Different calculations of the diameter dependence on the phonon frequencies for semiconducting SWCNTs, including a recent *ab initio* approach,¹⁷ point out the proximity of these $A(\text{LO})$ and $E_1(\text{TO})$ modes, especially in the diameter range investigated in this study. (ii) The resolution of the $A(\text{TO})$, $E_1(\text{LO})$, and $E_2(\text{LO})$ modes in the $1550\text{--}1580\text{ cm}^{-1}$ range allows their dependence to be followed with an improved accuracy with respect to previous investigations.

It is obvious that the lines close to 1585 cm^{-1} do not become integrated into the semiconducting TM frequency versus d^{-1} plot (Figure 6, solid symbols). Recently, a significant shift of the TM bunch has been observed for isolated tubes under uniaxial strain.³² Under a strain of 1.65% the TM, located at 1590 cm^{-1} prior to straining, is lowered by 40 cm^{-1} , while the RBM remains almost unchanged. So, we can assume that some tubes suspended between pillars can be under strain. This assumption is in agreement with the concomitant observation of a strong RBM at 170 cm^{-1} and a strong TM at 1585 cm^{-1} . To confirm this assumption, Raman experiments on isolated tube under progressive strain are in progress. Another possibility would be to assign the 1585 cm^{-1} mode to the Raman signature of a metallic tube.²⁹ Because strong 170 cm^{-1} RBM and 1585

cm^{-1} TM have a strong intensity in a same spectrum, that means that the 2.41 eV excitation energy is inside the excitation window of both these modes. With regards to the resonance conditions the 170 cm^{-1} RBM is unambiguously assigned to the response of a semiconducting tube. The presence in a same spectrum of a semiconducting and a metallic tube implies that (i) the 2.41 eV excitation energy perfectly matches the $E_{33}^S + 0.021\text{ eV}$ (170 cm^{-1}) energy (in this assumption, the weak bands around 1562 and 1593 cm^{-1} should be assigned to the TM of the semiconducting tube, Figure 5.a2), (ii) in a same time, the excitation energy perfectly matches the $E_{11}^M + 0.196\text{ eV}$ (1585 cm^{-1}) energy (the diameter of the metallic tube is assumed around $1.1\text{--}1.2\text{ nm}$) or the $E_{22}^M + 0.196\text{ eV}$ energy (in this case the diameter of the metallic tube is assumed around 2 nm , less probable in our point of view). The same kind of arguments can be given to explain the concomitant observation of modes assigned to semiconducting and metallic tubes in the Raman spectrum of Figure 4.a2. However, this explanation is speculative, and the measurement of the excitation profile of the RBM and TM could enlighten this assignment.

V. Conclusion

We have performed a detailed Raman study of suspended (free-standing) SWCNTs. Intense radial breathing modes and tangential modes have been systematically measured on a large number of individual suspended nanotubes. The plot of the Figure 6 gives a coherent picture of the diameter dependence of the TM frequencies of these semiconducting tubes. However no information about the chiral angle of the nanotubes, and then no identification of their lattice structure, that is the (n,m) indices, can be obtained from these Raman data.

The present study has mainly allowed (i) determination of the precise dependence with the diameter of the frequency of the tangential modes and (ii) to confirm, and sometimes to correct, the symmetry assignment of the tangential modes.

As previously recalled, the ultimate way to know the Raman response of well-identified individual SWCNTs is to combine Raman and electron diffraction experiments on the same free-standing individual SWCNTs. The electron diffraction technique independently provides the lattice structure, that is the (n,m) indices, of individual SWCNT.³³ Using this approach, we have recently measured the RBM of nine well-identified (n,m) tubes.²⁰ By this way we have derived for the first time in a large diameter range (from 1.4 to 3 nm) the exact relation between the RBM frequency and the tube diameter.²⁰ Analyses of the TM range measured on the same well-identified (n,m) tubes are now in progress. These latter data will allow the intrinsic Raman response in the TM range of SWCNTs to be known as a function of their diameter and chirality. These latter results will be compared with the present data in order to confirm/contradict the conclusions drawn in this paper.

References and Notes

- (1) Dresselhaus, M. S.; Eklund, P. C. *Adv. Phys.* **2000**, *49*, 705 and references therein.
- (2) Milnera, M.; Kürti, J.; Hulman, M.; Kuzmany, H. *Phys. Rev. Lett.* **2000**, *84*, 1324.
- (3) Rols, S.; Righi, A.; Alvarez, L.; Anglaret, E.; Almairac, R.; Journet, C.; Bernier, P.; Sauvajol, J.-L.; Benito, A. M.; Maser, W. K.; Muñoz, E.; Martínez, M. T.; de la Fuente, G. F.; Girard, A.; Ameline, J.-C. *Eur. Phys. J. B* **2000**, *18*, 202.
- (4) Pimenta, M. A.; Marucci, A.; Empedocles, S.; Bawendi, M.; Hanlon, E. B.; Rao, A. M.; Eklund, P. C.; Smalley, R. E.; Dresselhaus, G.; Dresselhaus, M. S. *Phys. Rev. B* **1998**, *58*, R16016.
- (5) Kataura, H.; Kumazawa, Y.; Maniwa, Y.; Umez, I.; Suzuki, S.; Ohtsuka, Y.; Achiba, Y. *Synth. Met.* **1999**, *103*, 2555.

- (6) Alvarez, L.; Righi, A.; Rols, S.; Anglaret, E.; Sauvajol, J.-L. *Chem. Phys. Lett.* **2000**, *320*, 441.
- (7) Brown, S. D.; Jorio, A.; Corio, P.; Dresselhaus, M. S.; Dresselhaus, G.; Saito, R.; Kneipp, K. *Phys. Rev. B* **2001**, *63*, 155414.
- (8) Kempa, K. *Phys. Rev. B* **2002**, *66*, 195406.
- (9) Paillet, M.; Ph. Poncharal, Zahab, A.; Sauvajol, J.-L.; Meyer, J. C.; Roth, S. *Phys. Rev. Lett.* **2005**, *94*, 237401.
- (10) Maultzsch, J.; Reich, S.; Schlecht, U.; Thomsen, C. *Phys. Rev. B* **2002**, *65*, 233402.
- (11) Marty, L.; Bouchiat, V.; Naud, C.; Chaumont, M.; Fournier, T.; Bonnot, A. M. *Nano Lett.* **2003**, *3*, 1115.
- (12) Marty, L. PhD Thesis, University of Grenoble, 2004.
- (13) Kobayashi, Y.; Yamashita, T.; Ueno, Y.; Niwa, O.; Homma, Y.; Ogino, T. *Chem. Phys. Lett.* **2004**, *386*, 153.
- (14) Saito, R.; Takeya, T.; Kimura, T.; Dresselhaus, G.; Dresselhaus, M. S. *Phys. Rev. B* **1998**, *57*, 4145.
- (15) Rahmani, A.; Sauvajol, J. L.; Rols, S.; Benoit, C. *Phys. Rev. B* **2002**, *66*, 125404.
- (16) Saito, R.; Jorio, A.; Hafner, J. H.; Lieber, C. M.; Hunter, M.; McClure, T.; Dresselhaus, G.; Dresselhaus, M. S. *Phys. Rev. B* **2001**, *64*, 85312.
- (17) Dubay, O.; Kresse, G.; Kuzmany, H. *Phys. Rev. Lett.* **2002**, *88*, 235506.
- (18) Kahn, D.; Ping Lu, J. *Phys. Rev. B* **1999**, *60*, 6535.
- (19) Rahmani, A. Private communication.
- (20) Meyer, J. C.; Paillet, M.; Moreac, A.; Neumann, A.; Duesberg, G. S.; Roth, S.; Sauvajol, J.-L. *Phys. Rev. Lett.* **2005**, *95*, 217401.
- (21) Jorio, A.; Saito, R.; Hafner, J. H.; Lieber, C. M.; Hunter, M.; McClure, T.; Dresselhaus, G.; Dresselhaus, M. S. *Phys. Rev. Lett.* **2001**, *86*, 1118.
- (22) Fantini, C.; Jorio, A.; Souza, M.; Strano, M. S.; Dresselhaus, M. S.; Pimenta, M. A. *Phys. Rev. Lett.* **2004**, *93*, 147406.
- (23) Telg, H.; Maultzsch, J.; Reich, S.; Henrich, F.; Thomsen, C. *Phys. Rev. Lett.* **2004**, *93*, 177401.
- (24) Jorio, A.; Pimenta, M. A.; Souza Filho, A. G.; Samsonidze, Ge., G.; Swan, A. K.; Ünlu, M. S.; B Goldberg, B.; Saito, R.; Dresselhaus, G.; Dresselhaus, M. S. *Phys. Rev. Lett.* **2003**, *90*, 107403.
- (25) Tan, P.-H.; Deang, Y.; Zhao, Q. *Phys. Rev. B* **1998**, *58*, 5435.
- (26) Huang, F.; Yue, K. T.; Tan, P.; Zhang, S.-L. *J. Appl. Phys.* **1998**, *84*, 4022.
- (27) Tan, P.-H.; An, L.; Liu, L.-Q.; Guo, Z.-X.; Czerw, R.; Caroll, D. L.; Ajayan, P. M.; Zhang, N.; Guo, H. L. *Phys. Rev. B* **2002**, *66*, 245410.
- (28) Souza, M.; Jorio, A.; Fantini, C.; Neves, B. R. A.; Pimenta, M. A.; Saito, R.; Ismach, A.; Joselevich, E.; Brar, V. W.; Samsonidze, Ge., G.; Dresselhaus, G.; Dresselhaus, M. S. *Phys. Rev. B* **2004**, *69*, 241403(R).
- (29) Fantini, C.; Pimenta, M. A.; Dantas, M. S. S.; Ugarte, D.; Rao, A. M.; Jorio, A.; Dresselhaus, G.; Dresselhaus, M. S. *Phys. Rev. B* **2001**, *63*, 161405.
- (30) Duesberg, G. S.; Loa, I.; Burghard, M.; Syassen, K.; Roth, S. *Phys. Rev. Lett.* **2000**, *85*, 5436.
- (31) Anglaret, E.; Righi, A.; Sauvajol, J.-L.; Bernier, P.; Vigolo, B.; Poulin, P. *Phys. Rev. B* **2002**, *65*, 165426.
- (32) Cronin, S. B.; Swan, A. K.; Ünlu, M. S.; Goldberg, B. B.; Dresselhaus, M. S.; Tinkham, M. *Phys. Rev. Lett.* **2004**, *93*, 167401.
- (33) Meyer, J. C.; Paillet, M.; Duesberg, G. S.; Roth, S. *Ultramicroscopy*, in press.